COBEM2015

ABCM Associação Brasileira de Engenharia e Ciências Mecânicas

23rd ABCM International Congress of Mechanical Engineering
December 6-11, 2015, Rio de Janeiro, RJ, Brazil

DESCRIPTION AND APPLICATION OF THE SCRAMJET ENGINE SIMULATION PACK(SJETSP)

Tiago Cavalcanti Rolim
Paulo Gilberto de Paula Toro
Divisão de Aerotermodinâmica e Hipersônica, Instituto de Estudos Avançados, Trevo Cel. Av. J. A. A. do Amarante, no. 1, Putim, São José dos Campos, São Paulo, Brasil, Cep. - 12.228-001.
tiagorolim@ieav.cta.br / tiagocrolim@outlook.com
toro@ieav.cta.br

Abstract. *A numerical model was developed for preliminary analysis of 2D scramjet engines. The advantage of the SJETSP is that it is capable of estimating a multitude of scramjet performance parameters with a short computational time. To achieve this, the inlet was modeled with the oblique shockwave relationships. The isolator, combustor and nozzle were treated using a quasi-one-dimensional, viscous and reacting flow model. The viscous effects were taken into account estimating the skin friction coefficient and the heat flux through the walls. A hydrogen-air combustion mechanism was also included along with a mixing model. Experiments were used to validate the numerical code and overall good agreement was achieved. Following, as a primary application, a baseline scramjet configuration was used to investigate how selected flow properties vary with different prescribed trajectories and fuel injection strategies. These studies revealed that the combustor flow properties are highly sensitive to changes in freestream properties and fuel-air equivalence ratio. Also, based on the results, general directions for the combustor design were made.*

Keywords: *Propulsion, hypersonics, scramjets, combustion*

1. INTRODUCTION

Because of the difficulty to reproduce the hypersonic flight conditions in ground facilities, mainly due to the high specific enthalpy associated, engineering models could provide a preliminary analysis of the flow inside the scramjet engine with a low cost. Also, these models can estimate a multitude of performance parameters with a relatively short computational time. Indeed, the design of tip-to-tail computational tools for scramjet flow analysis has been also an important matter of research (Dalle *et al.*, 2012).

In this work, we developed a methodology that utilizes oblique shockwave relationships to describe inlet properties and a quasi-one-dimensional model, with viscous effects evaluation, finite-rate chemistry, and a mixing law for the reactive flow inside isolator, combustor and nozzle. Results from this model were compared with experiments with a hydrogen-fueled scramjet.

Finally, we simulated an inward scramjet engine under two cruise velocities, 2.0 and 2.5 km/s, at 30 km of altitude, to study how selected flow properties change as freestream velocity changes. A secondary parameter involved on this study was the fuel–air equivalence ratio.

2. NUMERICAL MODELING

The following subsections describe the numerical models adopted for the inlet, isolator, combustor and nozzle flows. The nomenclature used for the scramjet engine is shown in Fig. 1. Stations 0 to 2 denote the inlet region, station 2 is the isolator entrance, station 3 is the combustor entrance, station 4 is the combustor exit and station 10 is the nozzle exit plane.

2.1 INLET (STATIONS 0–2)

Assuming a steady, inviscid and adiabatic flow, with a calorically perfect gas model, oblique shockwave relationships can easily be applied to retrieve flow properties along the inlet; for instance, the pressure, density and temperature ratios across each shockwave are

$$p_{ratio} = 1 + \frac{2\gamma_0}{\gamma_0 + 1}[M^2 \sin^2 \beta - 1] \tag{1}$$

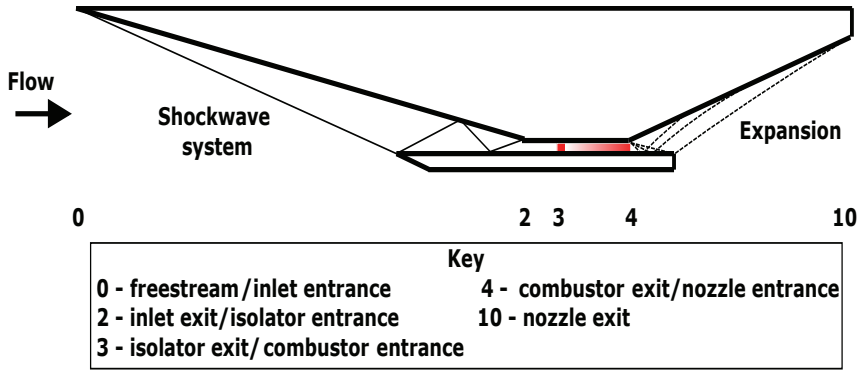

Figure 1: Scramjet schematics and reference stations.

and,

$$\rho_{ratio} = \frac{(\gamma_0 + 1)M^2 \sin^2 \beta}{2 + (\gamma_0 - 1)M^2 \sin^2 \beta} \tag{2}$$

Also,

$$T_{ratio} = p_{ratio}/\rho_{ratio} \tag{3}$$

where γ_0 is ratio of specific heats, M is the local Mach number and β is the shockwave angle with respect to the local flow direction, obtained iteratively with the relationship

$$\tan\theta = \frac{2\cot\beta[M^2\sin^2\beta - 1]}{M^2[\gamma_0 + \cos(2\beta)] + 2} \tag{4}$$

where θ is the flow deflection across the shockwave.

Since it was assumed an adiabatic flow and a calorically perfect gas model, one can get the flow velocity via:

$$V = \sqrt{2(h_{t0} - c_{p0}T)} \tag{5}$$

where h_{t0} is the freestream total specific enthalpy and c_{p0} is the freestream specific heat at constant pressure.

2.2 ISOLATOR, COMBUSTOR AND NOZZLE (STATIONS 2–10): QUASI-ONE-DIMENSIONAL VISCOUS AND REACTIVE FLOW

The variation of flow properties along the transverse direction of these components were considered relatively small compared to the axial variation, therefore, quasi-one-dimensional flow was assumed. Boundary layer effects were simplified using the Van Driest II approximation (Cebeci and Bradshaw, 1984) for the turbulent skin friction coefficient and viscous heating was calculated by use of the Reynolds analogy. Combustion reaction that takes place with the supersonic air exiting the inlet and the injected fuel is modeled by a finite rate chemistry with the H_2–air kinetic mechanism of Jachimowski (Jachimowski, 1988), which has 33 reactions and 13 species, with 9 third body reactions. Also, the thermodynamic properties of each species were calculated using the JANAF tables (Stull and Prophet, 1971). The fuel–air mixing law was according to Northam and Anderson model (Northam and Anderson, 1986) along with an assumed uniform fuel-mass injection profile.

2.2.1 FLUID CONSERVATION EQUATIONS

Considering a steady, quasi-one-dimensional and viscous flow, without body forces, no shaft work, and with a negligible work done by viscous forces, with the use of the differential fluid element shown in Fig. 2, one can show that, since mass is being injected into the system, mass conservation equation takes the form:

$$\frac{1}{\dot{m}}\frac{d\dot{m}}{dx} = \frac{1}{\rho}\frac{d\rho}{dx} + \frac{1}{u}\frac{du}{dx} + \frac{1}{A}\frac{dA}{dx} \tag{6}$$

where $\dot{m}$ is the mass flow rate, $d\dot{m}/dx$ is the fuel mass injection profile, u is the axial component of the flow velocity, and $A = A(x)$ is the cross-sectional area distribution.

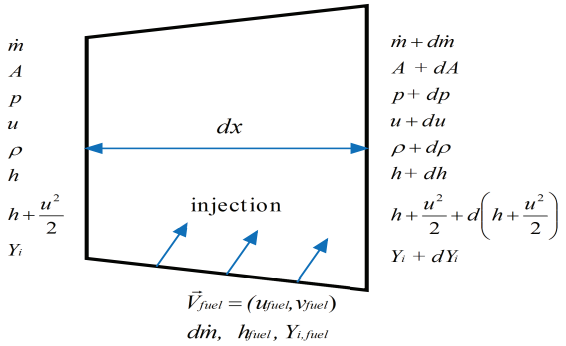

Figure 2: Differential element for the reacting flow analysis.

The axial momentum conservation applied onto the same differential element yields:

$$\rho u\frac{du}{dx}+\frac{1}{A}(u-u_{fuel})\frac{d\dot{m}}{dx}+\frac{dp}{dx}=\rho f \tag{7}$$

where u_{fuel} is the axial component of the fuel velocity and f is the total force produced by viscous effects per unit mass in the axial direction, given by:

$$f=-\frac{2}{D}u^2 c_f \tag{8}$$

where D is the hydraulic diameter and c_f is the skin friction coefficient.

Following, the the energy conservation applied in this component can be written as:

$$\dot{m}\frac{dh}{dx}=\left(h_{fuel}-h+\frac{\vec{V}_{fuel}^2}{2}-\frac{u^2}{2}\right)\frac{d\dot{m}}{dx}-\dot{m}u\frac{du}{dx}+(\rho A)\dot{q} \tag{9}$$

where h is the specific enthalpy of the mixture, h_{fuel} is the specific enthalpy of the fuel, $\vec{V}_{fuel}$ is the fuel velocity, and $\dot{q}$ is the heat transferred to the flow per unit mass per unit time. Considering that heat is lost just through the walls, one can show that:

$$\dot{q}=-\frac{4}{D\rho}\dot{q}_w \tag{10}$$

where $\dot{q}_w$ is the wall heat flux due to the boundary-layer, given by:

$$\dot{q}_w=c_H\rho u c_p(T_{aw}-T_w) \tag{11}$$

where c_H is the Stanton number, c_p is the mixture specific heat at constant pressure, T_{aw} is the adiabatic wall temperature and T_w is the wall temperature.

2.2.2 BOUNDARY LAYER

The skin friction coefficient was calculated using the Van Driest II equation, considering a turbulent flow. The recovery factor is given by $r=\mathrm{Pr}^{\frac{1}{3}}$ (Schlichting, 1979), while we assumed $\mathrm{Pr}=0.71$ constant. Species viscosities were evaluated using the Sutherland's law (Anderson, 2007) and the gas mixture viscosity was calculated using the Wilke's method (Wilke, 1950).

The heat flux through the walls for turbulent boundary layers can be estimated with a Reynolds analogy factor given by (Cebeci and Bradshaw, 1984):

$$\frac{c_H}{c_f/2}=1.16 \tag{12}$$

2.2.3 EQUATION OF STATE

In the case of a reacting flow, the equation of state $p=\rho RT$ can be differentiated, since the flow properties are varying along the combustor longitudinal coordinate. Thus,

$$\frac{1}{p}\frac{dp}{dx}=\frac{1}{\rho}\frac{d\rho}{dx}+\frac{1}{R}\frac{dR}{dx}+\frac{1}{T}\frac{dT}{dx} \tag{13}$$

where R is the gas constant.

2.2.4 CHEMICAL KINETICS

With the Jachimowski mechanism, the forward reaction constants were calculated for each reaction j according to the modified Arrhenius temperature relation:

$$k_{f_j} = \kappa_j T^{\chi_j} \exp(-\epsilon_j / T) \tag{14}$$

where κ_j, χ_j and ϵ_j are given constants.

The rate of progress variable for each reaction is given by:

$$\dot{\omega}_j = \left(k_{f_j} \Pi_{i=1}^{NS} W_i^{\nu'_{ij}} - k_{rj} \Pi_{i=1}^{NS} W_i^{\nu''_{ij}} \right) \tag{15}$$

where ν'_{ij} and ν''_{ij} are the stoichiometric indexes for each species i whether they are reactants or products in reaction j, respectively, and NS is the total number of species, W_i is the molar concentration of species i. Also, the backward rate constants were calculated via:

$$k_{rj} = k_{f_j} / k_{cj} \tag{16}$$

the molar concentration based equilibrium constant for each reaction, k_{cj}, was calculated using JANAF tables.

For the three body reactions, the rate of progress variable is given by:

$$\dot{\omega}_j = \sum_{i=1}^{NS} [\alpha_{ij} W_i] \left(k_{f_j} \Pi_{i=1}^{NS} W_i^{\nu'_{ij}} - k_{rj} \Pi_{i=1}^{NS} W_i^{\nu''_{ij}} \right) \tag{17}$$

where α_{ij} is the third body efficiency. Thus, for each species in the mechanism, the net rate of change of the molar concentration is given by:

$$\dot{W}_i = \sum_{j=1}^{NR} (\nu''_{ij} - \nu'_{ij}) \dot{\omega}_j \tag{18}$$

where NR is the total number of reactions of the chemical mechanism.

Since the flow is reactive, one can relate the specific enthalpy variation with the gas temperature and chemical composition variations via (Anderson, 1990):

$$dh = c_p dT + \sum_{i=1}^{NS} h_i dY_i \tag{19}$$

where Y_i is the species mass fraction and the mixture specific heat is calculated with,

$$c_p = \sum_{i=1}^{NS} c_{p_i} Y_i \tag{20}$$

The mixture gas constant can be obtained via:

$$R = \mathbf{R} \sum_{i=1}^{NS} Y_i / MW_i \tag{21}$$

where $\mathbf{R} = 8.314$ J/(mol·K) and MW_i is the species molecular weight. Differentiating this last relation, one can get:

$$\frac{dR}{dx} = \mathbf{R} \sum_{i=1}^{NS} \frac{1}{MW_i} \frac{dY_i}{dx} \tag{22}$$

With the fluid element of Fig. 2, the mass conservation for each species can be expressed by the differential equation (O'brien *et al.*, 2001),:

$$\frac{dY_i}{dx} = \frac{\dot{W}_i MW_i}{\rho u} + \frac{1}{\dot{m}} \frac{d\dot{m}}{dx} (Y_{i,fuel} - Y_i) \tag{23}$$

2.2.5 FUEL-MASS INJECTION

It was considered that the total fuel mass flow rate $\dot{m}_{fuel}$ was injected uniformly through all existent injectors and the fuel properties are constant along injectors exit plane. For the case of circular injectors, one can use:

$$\frac{d\dot{m}}{dx} = \frac{\dot{m}_{fuel}}{\pi d_{inj}^2/4}\frac{dA_{inj}}{dx} \tag{24}$$

where d_{inj} is the injector diameter, A_{inj} is the injector area, and

$$\frac{dA_{inj}}{dx} = d_{inj}\sqrt{1-4\frac{(x-x_{inj})^2}{d_{inj}^2}} \tag{25}$$

for $x_{inj} - \frac{d_{inj}}{2} \leq x \leq x_{inj} + \frac{d_{inj}}{2}$, where x_{inj} is the injection position.

2.2.6 MIXING

In this work, the mixing model of Northam and Anderson (Northam and Anderson, 1986) was adopted. The injection of fuel on the main air flow is modeled by means of the mixing efficiency parameter η_{mix}, defined as the ratio of the amount of fuel available for reaction to the total amount of injected fuel. Northam and Anderson pointed out that mixing efficiency can be estimated as a function of the distance from the injection point x_{inj} and the distance at which the fuel is completely mixed L_{mix}. They suggest, for the case of parallel injection:

$$\eta_{mix0^o} = (x - x_{inj})/L_{mix} \tag{26}$$

and, for the case of perpendicular injection:

$$\eta_{mix90^o} = 1.01 + 0.176\ln[(x - x_{inj})/L_{mix}] \tag{27}$$

Also, they suggest for injection angles between 0 and 90 deg. the mixing efficiency can be calculated using a linear interpolation between η_{mix0^o} and η_{mix90^o}. In this model, the distance at which the fuel is completed mixed is estimated by:

$$L_{mix} = \begin{cases} 0.179\ C_m\ d_{x_{inj}}\exp(1.72\phi_0), & \phi_0 \leq 1 \\ 3.33\ C_m\ d_{x_{inj}}\exp(-1.204\phi_0), & \phi_0 > 1 \end{cases} \tag{28}$$

where $C_m = 60$, ϕ_0 is the overall equivalence ratio and $d_{x_{inj}}$ is the duct size at injection point.

Thus, the fuel parcel which is accounted for the chemical kinetics mechanism, through Eqs. (15) and (17), is given by:

$$W_{\mathrm{H_2}} = \eta_{mix}\frac{\rho Y_{\mathrm{H_2}}}{MW_{\mathrm{H_2}}} \tag{29}$$

2.2.7 NUMERICAL SOLUTION

The set of equations presented in the previous subsections needed to be rearranged for proper numerical integration. To achieve this, first we use Eq.(9) combined with Eq.(19) to yield,

$$\frac{dT}{dx} = \frac{1}{c_p}\left[\frac{1}{\dot{m}}\frac{d\dot{m}}{dx}\left(h_{fuel} + \frac{\vec{V}_{fuel}^2}{2} - h - \frac{u^2}{2}\right) - \sum_{i=1}^{NS} h_i\frac{dY_i}{dx} - u\frac{du}{dx} + \frac{\dot{q}}{u}\right] \tag{30}$$

Moreover, one can solve Eq.(13) for dp/dx, substitute in Eq.(7), use Eq.(6) to eliminate $d\rho/dx$ and Eq.(30) to eliminate dT/dx and get:

$$\begin{aligned}\frac{du}{dx} = {} & \frac{1/u}{\frac{R}{c_p} + \frac{RT}{u^2} - 1}\left[\frac{u^2}{\dot{m}}\frac{d\dot{m}}{dx}\left(1 - \frac{u_{fuel}}{u}\right) - f + RT\left(-\frac{1}{A}\frac{dA}{dx} + \frac{1}{R}\frac{dR}{dx} + \frac{1}{\dot{m}}\frac{d\dot{m}}{dx}\right)\right] + \\ & \frac{R/(c_p\,u)}{\frac{R}{c_p} + \frac{RT}{u^2} - 1}\left[\frac{1}{\dot{m}}\frac{d\dot{m}}{dx}\left(h_{fuel} + \frac{\vec{V}_{fuel}^2}{2} - h - \frac{u^2}{2}\right) - \sum_{i=1}^{NS} h_i\frac{dY_i}{dx} + \frac{\dot{q}}{u}\right]\end{aligned} \tag{31}$$

Because the reaction rates can have vastly different timescales, the system of equations which model the flow inside the combustor was numerically integrated with an algorithm capable of dealing with stiff differential equations (Shampine and Reichelt, 1997). The step size was constant and equal to 10^{-5} m. A typical simulation time was about 212 s, using a 2.20 GHz processor with 8 GB of RAM.

2.3 STRUCTURE OF SJETSP

The numerical code was developed in MATLAB/Simulink platform (MATLAB, 2010). Each component of the scramjet engine was modeled with a MATLAB function and corresponds to a single block in Simulink environment, where the blocks were connected, see Fig. 3. The code has sub-folders containing functions that models oblique shockwaves, boundary-layer, chemical kinetics, mixing model, thermodynamic properties, and a quasi-one-dimensional flow solver.

With the use of Aerospace Blockset to obtain freestream properties, each simulation time corresponds to a trajectory point. The inputs are the trajectory file, which contains a vector of all velocities and altitudes to be simulated, the wall temperature in each component, and there is also a block for input of injection parameters: fuel-air equivalence ratio, injector diameter, injection angle, and fuel reservoir temperature. The geometry of the isolator-combustor and nozzle, which are modeled with a quasi-one-dimensional assumption, are given by a separate file.

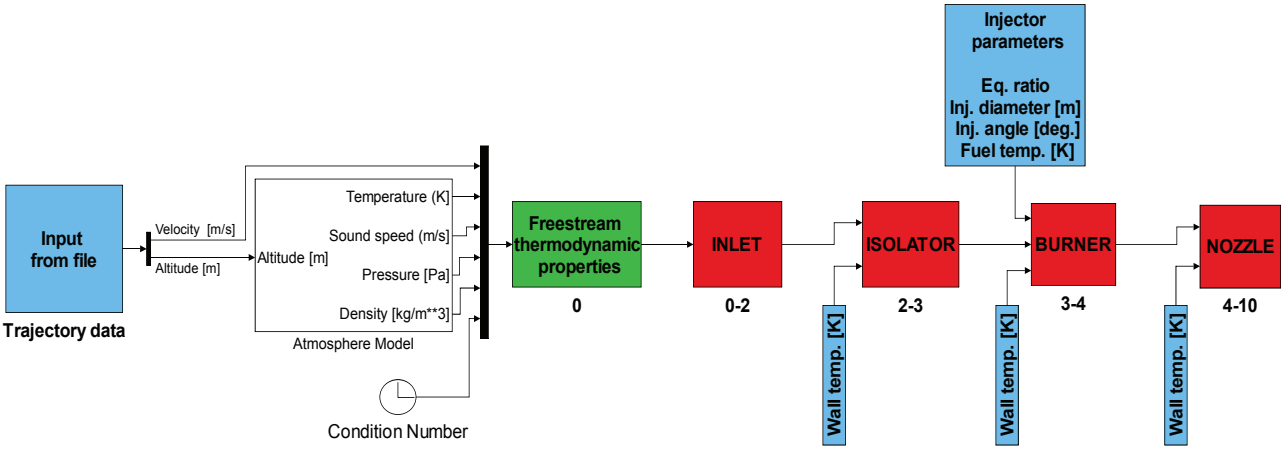

Figure 3: Simulink model of SJETSP.

3. RESULTS

3.1 CODE VALIDATION

To study the accuracy of the SJETSP, comparisons have been made between numerical results and those obtained by experiments in ground facilities. For instance, validation was performed using the model from Kang, Lee, Yang, Smart and Suraweera (Kang *et al.*, 2010, 2007), a two-dimensional scramjet with design Mach number of 7.6, with geometry described in Fig. 4, which has a constant width of 0.100 m. In the work presented by Kang et al., the freestream conditions were Mach number of 7.56, p_0 = 0.0109 atm, T_0 = 243 K and γ_0 = 1.39. The wall temperature was kept in 300 K. The hydrogen was injected with an angle of 45 deg., with injector hole diameters of 2 mm, also on a temperature of 300 K. Among all fuel equivalence ratios investigated in that work, we chose the cases of ϕ_0 = 0.18 and 0.11. For the calculations, the engine was separated in two parts. In the first part, from x = 0 to 0.5768 m, the inlet external compression, we used the model described in Sec. 2.1, considering oblique shockwaves with deflection angles of 12, 15 and 12 deg. From x = 0.5768 to 0.9575 m, the quasi-one-dimensional assumption was adopted, according to Sec. 2.2. The air composition entering engine was assumed as Y_{N_2} = 0.7655 and Y_{O_2} = 0.2345.

The pressure distributions are presented on Figs. 5a and 5b, for the two different cases, respectively. As it is shown in those figures, the calculated values and the experimental results are in a good overall agreement. On the inlet region, the pressure rise near x = 0.400 m observed on experiments is due to a separation zone at the beginning of the second ramp. However, as pointed out by Kang et al., the size of this separation zone was not large enough to affect the downstream flow. For both cases, at the inlet exit, the numerical data showed a more complex pressure distribution resulting from the cowl shockwave near x = 0.5768 m.

Furthermore, slight differences were observed at the injection point x = 0.6156 m, which are mostly due to shock-shock and shock-expansion interactions not modeled by the proposed methodology. On the other hand, the fuel mass injection position was characterized by a small pressure rise caught only in the numerical method. The model predicts well the position of the steeper pressure rise which characterizes the combustion reaction. Analysis of OH mass fraction distribution, also shown in Figs. 5a and 5b, indicates that the OH peak, considered as mixture ignition criterion, occurred near x = 0.7134 m, $Y_{OH} = 3.63 \times 10^{-3}$, when ϕ_0 = 0.18; and x = 0.7270 m, $Y_{OH} = 2.02 \times 10^{-3}$, for ϕ_0 = 0.11, both in agreement with pressure data from experiments which suggests that ignition takes place close to x = 0.6895 m, a difference of less than 4% and 6%, respectively. Discrepancies found in the pressure distribution along the engine

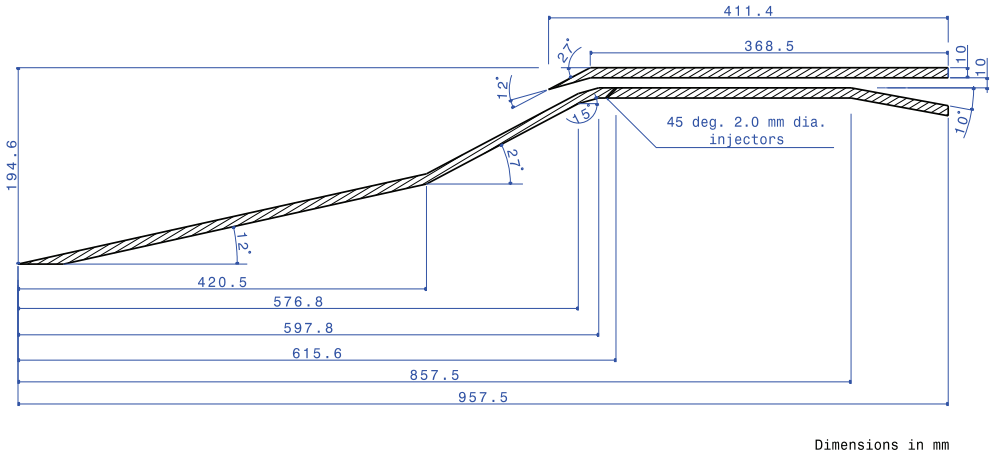

Figure 4: Schematics of the model used in the experiments of Kang (2010).

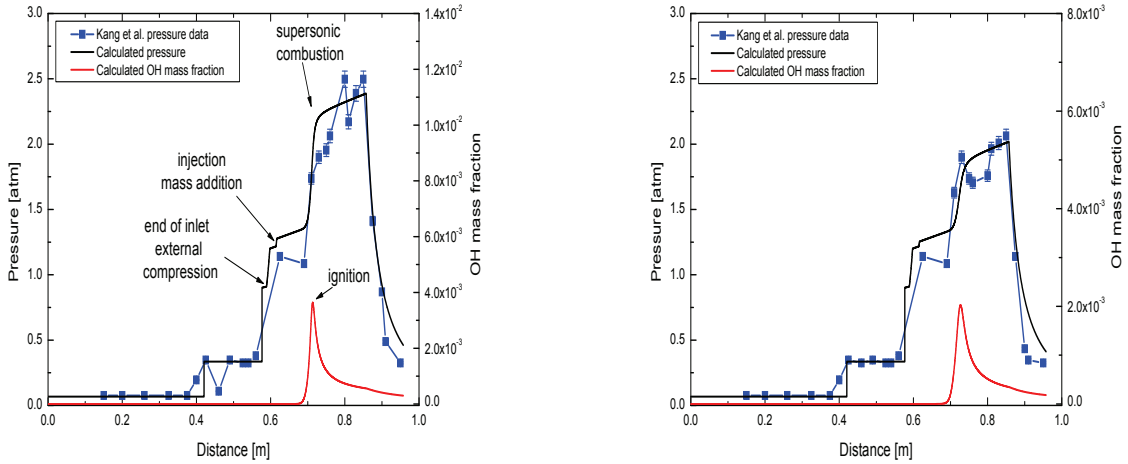

(a) $\phi_0 = 0.18$ (b) $\phi_0 = 0.11$

Figure 5: Comparison of numerical analysis and experimental data of Kang (2010).

combustor, from x = 0.5978 to 0.8575 m, might be due to the shock-train inside the combustor which is not accounted in our quasi-one-dimensional analysis. Also, differences might arise because shock-wave/boundary-layer interactions occur inside the combustor. Despite that, experimental data showed that the maximum pressure achieved was 2.50 atm at x = 0.8500 m close to 2.38 atm, calculated at that same position, for the case of ϕ_0 = 0.18, a relative difference of less than 5%. In the ϕ_0 = 0.11 case, the maximum pressure in the experimental data was 2.01 atm at x = 0.8500 m against a calculated pressure of 2.00 atm at the same position, a relative difference of less than 1%. At the expansion portion from x = 0.8575 to 0.9575 m, good agreement was achieved at the first stations. However, the computed pressure at x = 0.9500 m, the last experimental station, was 0.50 and 0.44 atm, for the cases ϕ_0 = 0.18 and 0.11, respectively, while the experiment shows a value of 0.33 atm for both cases. These discrepancies might be due to the accumulated error from the growing boundary layer and the existence of a centered expansion fan on the last ramp of the combustor, which increases flow angularity at the exit plane.

3.2 APPLICATION: FREESTREAM VELOCITY AND EQUIVALENCE RATIO EFFECTS

As an application and also to explore the developed numerical code, the effects of the equivalence ratio were investigated utilizing an inward scramjet model of Fig. 6. This scramjet configuration has a design velocity of 2.0 km/s at 30 km of altitude, the flow is decelerated by the shock-waves generated at the leading-edges and their reflections on the inlet walls, the contraction ratio (CR) is 17.5. Details of the inlet design can be seen elsewhere (Rolim and Lu, 2013; Vilela *et al.*, 2013). This configuration has a 0.300 m length combustor. The combustor height increases from 0.0114 to 0.014 m, a divergence angle of 0.497 deg. in lower wall. The hydrogen is injected through 2.0 mm diameter holes at 60 deg. angle with respect to the main flow direction. The nozzle has a symmetric expansion region of 0.400 m, with a divergence half angle of 14 deg. The engine has a constant width of 0.100 m.

For the simulations, we considered two cases: in the first one, the freestream velocity was 2.0 km/s (design point) and in the second one, we consider a velocity of 2.5 km/s (off-design), both at a constant altitude of 30 km, so the flight Mach number was 6.64 and 8.30, respectively, see Table 1 for other freestream properties. Also, it was considered fuel-air

equivalence ratio values of 0.12 and 0.25. In all cases, the fuel and wall temperatures were assumed equal to 300 K.

Table 1: Freestream properties, at 30 km of altitude.

Property	Value	Units
p_0	0.0116	atm
T_0	226.65	K
γ_0	1.4	-
Y_{O_2}	0.2345	-
Y_{N_2}	0.7655	-
V_0	2.0 and 2.5	km/s

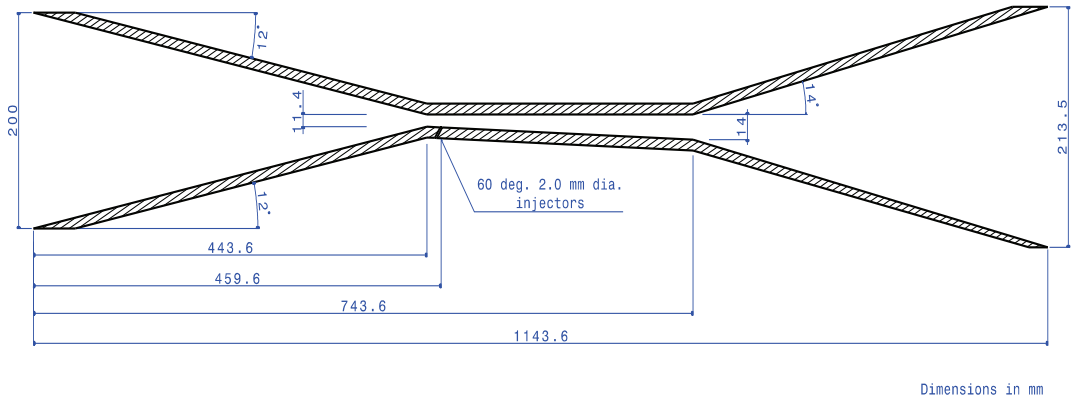

Figure 6: Adopted scramjet geometry.

To obtain the positions of the shockwave intersections and wall reflection points on engine inlet, it was considered the schematics of Fig. 7. After calculating each shockwave angle and the flow properties across them, one can retrieve the coordinates of points i, ii and iii solving the following system of equations:

$$\begin{aligned} &\bar{x}_i \tan\beta_i = 1 \\ &(\bar{x}_{ii} - \bar{x}_i)\tan(\beta_{ii} - \theta_w) = \bar{y}_{ii} \\ &\bar{x}_{ii}\tan\theta_w = 1 - \bar{y}_{ii} \\ &(\bar{x}_{iii} - \bar{x}_{ii})\tan\beta_{iii} = \bar{y}_{ii} \end{aligned} \tag{32}$$

where $\bar{x} = x/y_{LE}$ and $\bar{y} = y/y_{LE}$ are the dimensionless coordinates. As discussed before, downstream station 2 the flow was assumed to be quasi-one-dimensional.

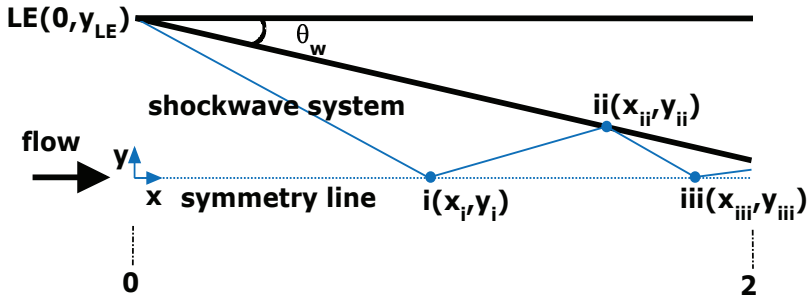

Figure 7: Scheme for obtaining the positions of shockwave intersection and reflection points on inlet.

The results from this simulation are shown in Figs. 8 and 9. Figure 8 shows the pressure distribution along engine. In that figure, one can notice that from stations x = 0 to 0.4436 m the oblique shockwave system originated at the inlet produces the multiple step pattern on pressure distribution. Also, the positions of the shockwave reflection points change with the freestream velocity.

The resulting pressure distributions are shown in Fig. 8, for the limiting cases V_0 = 2.0 and 2.5 km/s, using the two equivalence ratios. In Fig. 8, one can notice that from stations x = 0 to 0.4436 m the oblique shockwave system originated at the inlet produces the multiple step pattern on pressure distribution. Also, the positions of the shockwave reflection points change with the freestream velocity. At x = 0.4436 m, the inlet exit, the pressure was 1.26 and 2.41 atm, for the

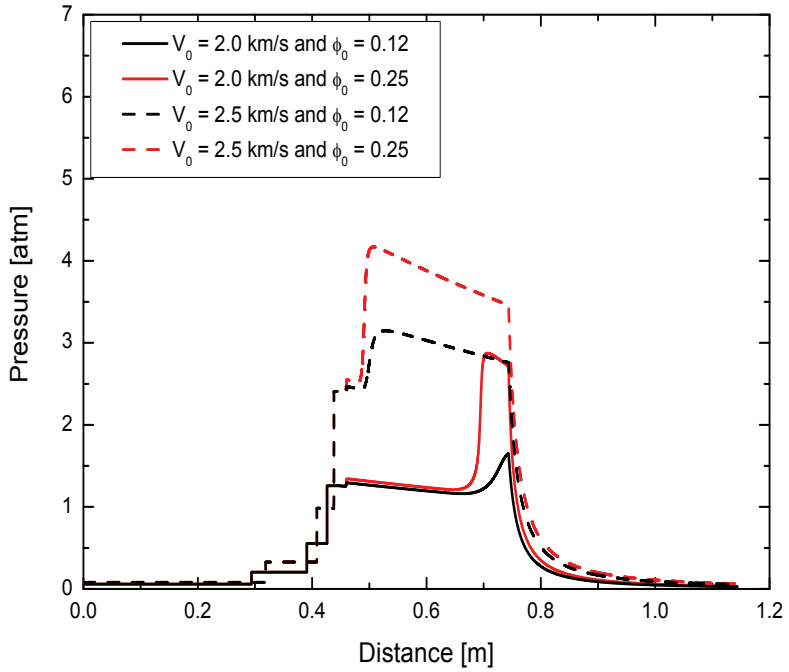

Figure 8: Pressure distribution along engine length, for V_0 = 2.0 and 2.5 km/s, for the cases of ϕ_0 = 0.12 and 0.25.

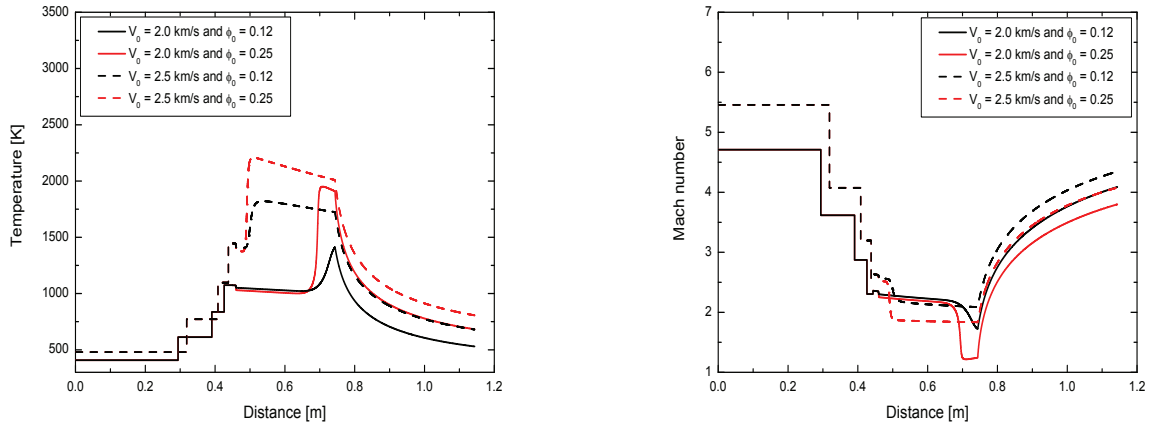

(a) Temperature (b) Mach number

Figure 9: Temperature and Mach number distributions from V_0 = 2.0 and 2.5 km/s, and ϕ_0 = 0.12 and 0.25.

cases of 2.0 and 2.5 km/s, respectively. Inside the combustor, the slight pressure rise near x = 0.4596 m characterizes the injection position. The flow expansion due to the combustor divergent geometry causes the pressure decrease observed in all cases. The steeper pressure rise downstream injection indicates the combustion reaction. The equivalence ratio and the velocity variation had a substantial influence on combustor pressure. However, the pressure at combustor exit was slightly more sensible to the velocity variation than to the equivalence ratio. For V_0 = 2.0 km/s, the calculated combustor exit pressure was 1.65 and 2.72 atm, for ϕ_0 = 0.12 and 0.25, respectively, a relative increase of 64.8%. When V_0 = 2.5 km/s, the combustor exit pressure varied from 2.76 to 3.46 atm (25.4%), as the equivalence ratio increases. On the other hand, for ϕ_0 = 0.12, the combustor exit pressure varied 67.3%, and 27.2%, for the case of ϕ_0 = 0.25, as velocity increases. Although more pronounced, a similar result was found at the nozzle exit pressure, the variation due to the freestream velocity was more significant than the variation due to the equivalence ratio. For ϕ_0 = 0.12, the pressure at x = 1.1436 m varied from 0.027 to 0.053 atm (96.3%) and from 0.034 to 0.063 atm (85.3%), when ϕ_0 = 0.25, as V_0 increases. Meanwhile, relative variations of only 25.9% and 18.9% were found, from ϕ_0 = 0.12 to 0.25, for the respective velocities of 2.0 and 2.5 km/s.

Fig. 9a shows the temperature distributions for the investigated equivalence ratios and for this same freestream velocity range. The temperature at combustor entrance varied from 1075 to 1446 K, as the freestream velocity was increased. Differently from the pressure, the temperature at combustor exit was more sensible to the equivalence ratio rather than to the velocity variation, this is due to fact that the temperature distribution is closely related to the heat released from the combustion reaction. In the case of V_0 = 2.0 km/s, the temperature at combustor exit, x = 0.7436 m, was 1414 K, for ϕ_0 = 0.12, against 1909 K, when ϕ_0 = 0.25, a relative increase of 35%. For V_0 = 2.5 km/s, the calculated combustor exit

temperature was 1724 K, in the ϕ_0 = 0.12 case, and 2009 K for ϕ_0 = 0.25, a relative difference of 16.5%. The nozzle exit temperature varied from 530 to 682 K, for V_0 = 2.0 km/s, and from 680 to 806 K, for V_0 = 2.5 km/s, as the equivalence ratio increases.

In Fig. 9b the Mach number distributions for the investigated cases are shown. At the inlet exit, the Mach number varied from 2.36 to 2.64. Despite the divergent geometry of the combustor, the Mach number at this component decreases as an effect of friction and combustion. The fuel ignition is characterized by a sharp Mach number decrease due to the high temperature associated, and if the heat release is large enough, thermal choking can occur inside the combustor. Thus, when analyzing Mach number distribution inside this component, one of the objectives is to track the minimum Mach number to prevent potential flow choking. For the cases when ϕ_0 = 0.12, the minimum Mach number position was at combustor exit, with values of 1.72 and 2.09, for V_0 = 2.0 and 2.5 km/s, respectively. However, when ϕ_0 = 0.25, the minimum Mach number position varied, a value of 1.22 was achieved at x = 0.7096 m, while the combustor exit Mach number was 1.24 for V_0 = 2.0 km/s. With this same equivalence ratio, the minimum Mach number moved to the combustor exit for V_0 = 2.5 km/s, with a value of 1.83. At nozzle exit, from V_0 = 2.0 to 2.5 km/s, the calculated Mach number had only a slight variation, from 4.09 to 4.35, for ϕ_0 = 0.12, and from 3.80 to 4.08, in the ϕ_0 = 0.25 case.

4. GENERAL RECOMMENDATIONS FOR THE COMBUSTOR DESIGN

Based on the present study, as general recommendations, the combustor design must consider different freestream conditions due to the large dependence of the hydrogen-air combustion mechanism on upstream properties. As a result of this fact, the overall performance of the scramjet varies considerably with changes of trajectory parameters, such as velocity. Thus, the knowledge of potential changes of freestream properties during flight is fundamental to a proper hypersonic airbreathing propulsion.

Furthermore, studies on the adopted scramjet configuration revealed that the equivalence ratio had a substantial influence on major combustor flow properties but relatively low influence on ignition position. These influences were attenuated as freestream velocity increases.

5. CONCLUSIONS

A numerical model was developed for preliminary analysis of 2D scramjet engines, the Scramjet Simulation Pack (SJETSP). This tool is capable of estimating a multitude of scramjet performance parameters using the Simulink/MATLAB platform. The inlet was modeled with the oblique shockwave relationships. The isolator, combustor and nozzle were treated using a quasi-one-dimensional, viscous and reacting flow model. The viscous effects were taken into account estimating the skin friction coefficient and the heat flux through the walls. A hydrogen-air combustion mechanism was also included along with a mixing model. Experiments were used to validate the numerical code and overall good agreement was achieved. Following, as a primary application, a baseline scramjet was simulated considering two conditions, 2.0 and 2.5 km/s at 30 km of altitude, to study how selected flow properties change as freestream velocity changes. A secondary parameter involved on this study was the fuel-air equivalence ratio.

6. REFERENCES

Anderson, J.D., 1990. *Modern Compressible Flow: with historical perspective*. McGraw-Hill, New York, 2nd edition.

Anderson, J.D., 2007. *Fundamentals of Aerodynamics*. McGraw-Hill, London, UK, 4th edition.

Cebeci, T. and Bradshaw, P., 1984. *Physical and Computational Aspects of Convective Heat Transfer*. Springer-Verlag, New York, NY.

Dalle, D.J., Torrez, S.M. and Driscoll, J.F., 2012. "Rapid Analysis of Scramjet and Linear Plug Nozzles". *AIAA Journal of Propulsion and Power*, Vol. 28, No. 3, pp. 545–555.

Jachimowski, C.J., 1988. "An Analytica1 Study of the Hydrogen-Air Reaction Mechanism With Application to Scramjet Combustion". TP 2791, NASA.

Kang, S.H., Lee, Y.J. and Yang, S.S., 2007. "Design of Model Scramjet Engine for Shock Tunnel Test". In *Proceedings of the 9th Asian International Conference on Fluid Machinery*. Seoul, South Korea.

Kang, S.H., Lee, Y.J., Yang, S.S., Smart, M. and Suraweera, M., 2010. "Cowl and Cavity Effects on Mixing and Combustion in Scramjet Engines". *AIAA Journal of Propulsion and Power*, Vol. 27, No. 6, pp. 1169–1177.

MATLAB, 2010. *version 7.10.0 (R2010a)*. The MathWorks Inc., Natick, Massachusetts.

Northam, G.B. and Anderson, G.Y., 1986. "Survey of Supersonic Combustion Ramjet at Langley". AIAA 86-0159.

O'brien, T.F., Starkey, R.P. and Lewis, M.J., 2001. "Quasi-One-Dimensional High-Speed Engine Model with Finite-Rate Chemistry". *AIAA Journal of Propulsion and Power*, Vol. 17, No. 6, pp. 1366–1374.

Rolim, T.C. and Lu, F.K., 2013. "Design and Stream Thrust Analysis of a Scramjet Engine for Acceleration Mission from 2 to 3 km/s". AIAA 2013-0120.

Schlichting, H., 1979. *Boundary-Layer Theory*. McGraw-Hill Series in Mechanical Engineering, New York, NY.

Shampine, L.F. and Reichelt, M.W., 1997. "The MATLAB ODE Suite". *SIAM Journal on Scientific Computing*, Vol. 18, pp. 1–22.

Stull, D.R. and Prophet, H., 1971. "JANAF Thermochemical Tables". Technical Report ADD095223, National Standard Reference Data System.

Vilela, R.G.S., Toro, P.G.P., Leite, V.S.F.O., Rolim, T.C. and Lu, F.K., 2013. "Inward 2-D Scramjet Analytic and Numerical Analysis at Mach Number 7 and Dimensional Design for Experimental Investigations". In *22nd International Congress of Mechanical Engineering (COBEM 2013)*. Brazilian Society of Engineering and Mechanical Sciences - ABCM, Ribeirao Preto, SP, Brazil.

Wilke, C.R., 1950. "A Viscosity Equation for Gas Mixtures". *The Journal of Chemical Physics*, Vol. 18, No. 4, pp. 517–519.

7. RESPONSIBILITY NOTICE

The authors are the only responsible for the printed material included in this paper.